

# A Robust Model Predictive Controller applied to a Pressure Swing Adsorption Process: An Analysis Based on a Linear Model Mismatch

Paulo H. M. Oliveira<sup>a</sup>, Márcio A. F. Martins<sup>\*a,b</sup>, Alírio E. Rodrigues<sup>a</sup>, José M. Loureiro<sup>a</sup>, Ana M. Ribeiro<sup>a</sup>, Idelfonso B. R. Nogueira<sup>\*a</sup>

<sup>a</sup>Laboratory of Separation and Reaction Engineering, Associate Laboratory LSRE-LCM  
Department of Chemical Engineering, Faculty of Engineering, University of Porto  
Rua Dr. Roberto Frias, 4200-465, Porto, Portugal.

<sup>b</sup>Departamento de Engenharia Química, Escola Politécnica (Polytechnic School),  
Universidade Federal da Bahia,  
R. Prof. Aristides Novis, 2 - Federação, 40210-630, Salvador - BA, Brazil.

*\*(e-mail: idelfonso@fe.up.pt; marciomartins@ufba.br)*

---

**Abstract:** The present work studies the control problem of a pressure swing adsorption (PSA) unit using a robust stabilizing infinite-horizon model predictive (RIHMPC) strategy with guarantee of feasibility for realistic mismatch scenarios. The identification of the multi-plant linear models was done based on an operating confidence region. This procedure is based on an optimal point given by an optimization layer, concomitantly with the uncertainty associated with that point. As a case study, it was evaluated the control of a PSA unit for the purification of syngas by porous amino-functionalized titanium terephthalate MIL-125 in the PSA. The results demonstrated that RIHMPC might be an efficient strategy to address the control of cyclic adsorption processes accommodating the intrinsic nonlinearities and uncertainties of these processes.

**Keywords:** Model Predictive Control, Robust Stability, Pressure Swing Adsorption, Model Uncertainty

---

## 1. INTRODUCTION

Pressure Swing Adsorption (PSA) processes are known for their capacity to promote efficiently complex gas phase separation. To perform the separation, they take advantage of the differences in the kinetics and/or equilibrium between the gases and solid phase. In order to play with the phenomenology of the system, the operation of these units is done in steps with specific roles. Consequently, those processes assume a periodic dynamic nature, in which no steady state is reached. This dynamic behavior corroborates to a series of issues found in the field, which are still open in the literature. The control of those units is one of these problems. Few works can be found in the literature addressing the control problem in PSA units. Most of those works address this problem using reduced-order models coped with model predictive control solutions (MPC) (Dias and Ierapetritou, 2019; Khajuria and Pistikopoulos, 2011; M. Mulholland, 2009; Rumbo Morales et al., 2020). In Dias and Ierapetritou (2019), in the control context, besides the system dynamics, the model identification is presented as one of the main challenges in the advanced control of the intensified process. On one hand, the first principle models for those processes are complex and associated with a heavy computational effort, which has limited their application to an offline scenario. On the other hand, the reduced-order models are limited to a short operating range, out of which their prediction starts to be unreliable.

In this context, to consider the model's uncertainty appears to be a good solution. It might allow the use of computationally efficient models while addressing their associated uncertainties. Therefore, the Robust Model Predictive Controller (RMPC) can be presented as a conciliative solution in the PSA control field. These controllers deal with systems whose several models can be used to represent the system under study. Among the RMPC literature, it is possible to highlight the structure proposed by Badgwell, (1997). In the referred work, the author extended the stabilizing infinite-horizon strategy to the robust scenario considering a multi-plant uncertainty description. Therefore, achieving asymptotic stability using a Lyapunov-like function and robust stability using terminal constraints. This strategy, known as Robust stabilizing infinite-horizon model predictive controller (RIHMPC), due to the above characteristics, has demonstrated its potential for practical implementation (Martins et al., 2014; Nogueira et al., 2020(1)).

The RIHMPC considers model uncertainty using a range of possible linear models in a multi-plant approach. Therefore, one of its core points is a discrete set of linear models used to represent the nonlinearities of the process. Thus, a methodology for the identification of these models needs to be defined.

Hence, the objective of this work is to present a RIHMPC applied in the control of a PSA unit, hitherto unexplored in the literature. In fact, as far as we know, stabilizing MPC strategies, including robust formulation to handle model

uncertainty, have not yet been reported in the literature, so this is an important contribution of the article. A strategy for the identification of linear models of the unit is also proposed, which is based on the uncertainty evaluation of an optimal point. As a case study, the purification of synthesis gas, syngas, is presented. This case study has great appeal to the energy industry, as the syngas is one of the main sources available for the production of pure H<sub>2</sub> and synthetic fuels.

## 2. MATHEMATICAL MODELS

### 2.1 Pressure Swing Adsorption

A rigorous model of the PSA unit was here used to identify the reduced-order models. The model for purification of syngas by porous amino-functionalized titanium terephthalate MIL-125 in the PSA was validated experimentally by Regufe et al. (2015). This model was based on the following assumptions: ideal gas behavior throughout the column; no mass, heat or velocity gradients in the radial direction; axial dispersed plug flow; external mass and heat transfer resistances expressed with the film model; internal mass transfer resistance expressed with the Linear Driving Force (LDF) model; no temperature gradients inside each particle since the heat transfer in the solid particles is much faster than in the gas phase; constant porosity along the bed; the Ergun equation is valid locally, i.e., in the momentum balance, only the terms of pressure drop and velocity change. The model, proposed by Da Silva et al., (1999), is composed by the following points.

#### Mass balance in the gas phase:

$$\frac{\partial}{\partial z} \left( \varepsilon D_{ax} C_{g,T} \frac{\partial y_i}{\partial z} \right) - \frac{\partial}{\partial z} (u_0 C_{g,i}) - \varepsilon \frac{\partial C_{g,i}}{\partial t} - (1 - \varepsilon) a_p k_f (C_{g,i} - C_{s,i}) = 0 \quad (1)$$

where  $z$  is the axial position,  $t$  is the time,  $\varepsilon$  is the bed porosity,  $u_0$  is the superficial velocity,  $C_{g,T}$  and  $C_{g,i}$  are respectively the total and component  $i$  gas-phase concentrations,  $y_i$  is the component  $i$  molar fraction,  $C_{s,i}$  is the concentration of component  $i$  at the solid interface,  $D_{ax}$  is the mass axial dispersion coefficient,  $k_f$  is the film mass transfer coefficient,  $a_p$  is the particle external specific area.

#### The pressure drop represented by the Ergun equation as:

$$-\frac{\partial P}{\partial z} = \frac{150\mu(1-\varepsilon)^2}{\varepsilon^3 d_p^2} u_0 + \frac{1.75(1-\varepsilon)\rho}{\varepsilon^3 d_p} |u_0| u_0 \quad (2)$$

with  $P$  as the total pressure,  $\mu$  as the gas viscosity,  $\rho$  as the gas density,  $d_p$  as the particle diameter.

#### The energy balance is given by:

$$\begin{aligned} \frac{\partial}{\partial z} \left( \lambda \frac{\partial T_g}{\partial z} \right) - u_0 C_{g,T} C_p \frac{\partial T_g}{\partial z} + \varepsilon R_g T_g \frac{\partial C_{g,T}}{\partial t} \\ - (1 - \varepsilon) a_p h_f (T_g - T_p) - \frac{4h_w}{d_{wi}} (T_g - T_w) \\ - \varepsilon C_{g,T} C_V \frac{\partial T_g}{\partial t} = 0 \end{aligned} \quad (3)$$

where,  $T_g$ ,  $T_p$  and  $T_w$  are respectively the gas; particle and wall temperatures  $C_v$  and  $C_p$  are the gas molar specific heats

at constant volume and pressure, respectively;  $R_g$  is the ideal gas constant;  $d_{wi}$  is the wall internal diameter;  $\lambda$  is the heat axial dispersion coefficient;  $h_f$  is the film heat transfer coefficient between the gas phase and the particle;  $h_w$  the heat transfer coefficient between the gas phase and the wall.

#### Linear driving force model (LDF) to represent the mass transfer rates in the solid phase:

$$\frac{\partial \bar{q}_i}{\partial t} = \frac{15D_{p,i}}{R_p^2} (q_i^* - \bar{q}_i) \quad (4)$$

where  $D_{p,i}$  is the pore diffusivity,  $R_p$  is the particle radius,  $\bar{q}_i$  is the particle averaged adsorbed concentration, and  $q_i^*$  is the adsorbed concentration in equilibrium with  $C_{s,i}$  calculated with the multicomponent extension.

#### Langmuir isotherm as:

$$q_i^* = q_{m,i} \frac{K_i P_i}{[1 + \sum_{j=1}^n K_j P_j]} \quad (5)$$

where  $K_j$  is the affinity constant. The isotherms parameters are given in Table 1.

**Table 1 - Langmuir parameters.**

Species	$q_m$ (mol·kg <sup>-1</sup> )	$K_i^0$ (bar <sup>-1</sup> )	$(-\Delta H)$ (kJ·mol <sup>-1</sup> )
CO <sub>2</sub>	8.509	$0.5782 \times 10^{-5}$	21.9
CO	5.229	$3.2700 \times 10^{-4}$	11.9
H <sub>2</sub>	0.294	$9.3900 \times 10^{-7}$	35.3

#### Fluxes equality at particle surface given by:

$$\frac{(1 - \varepsilon) a_p k_f}{\rho_b} (C_{g,i} - C_{s,i}) = \frac{15D_{p,i}}{R_p^2} (q_i^* - \bar{q}_i) \quad (6)$$

#### The solid phase energy balances are given by:

$$\begin{aligned} (1 - \varepsilon) \left[ \varepsilon_p \sum_{i=1}^n \bar{C}_{p,i} C_{v,i} + \rho_p \sum_{i=1}^n \bar{q}_i C_{v,ads,i} + \rho_p \hat{C}_{ps} \right] \frac{\partial T_p}{\partial t} \\ = (1 - \varepsilon) \varepsilon_p R_g T_p \frac{\partial \bar{C}_{p,T}}{\partial t} \\ + \rho_b \sum_{i=1}^n (-\Delta H_{ads})_i \frac{\partial \bar{q}_i}{\partial t} + (1 - \varepsilon) a_p h_f (T_g - T_p) \end{aligned} \quad (7)$$

where  $\rho_b$  is the bulk density of the bed;  $\hat{C}_{ps}$  is the solid specific heat per mass unit;  $(-\Delta H_{ads})_i$  is the heat of adsorption of component  $i$ .

#### The heat transfer through the wall is described as:

$$\rho_w \hat{C}_{p,w} \frac{\partial T_w}{\partial t} = \alpha_w h_w (T_g - T_w) - \alpha_{wi} U (T_w - T_\infty) \quad (8)$$

where  $T_{\infty}$  is the external temperature,  $\rho_w$  is the wall density,  $\hat{C}_{p,w}$  is the wall specific heat per mass unit,  $U$  is the overall heat transfer coefficient and  $e$  is the wall thickness.

$\alpha_w$  and  $\alpha_{wl}$  are defined as:

$$\alpha_w = \frac{d_{wl}}{e(d_{wl} + e)} \quad (9)$$

$$\alpha_{wl} = \frac{2}{(d_{wl} + e) \ln\left(\frac{d_{wl} + 2e}{d_{wl}}\right)} \quad (10)$$

The unit here presented considers 4 steps. The boundary conditions for each step of the PSA process are given in Table 2.

**Table 2 - Model boundary conditions.**

#### Pressurization with feed

$z = 0, \text{ inlet}$ $u_{0inlet} C_{inlet,i}$ $= u_0 C_{g,i} - \varepsilon D_{ax} C_{g,T} \frac{\partial y_i}{\partial z}$ $P = P_{inlet}$ $u_{0inlet} C_{inlet,T} C_p T_{inlet}$ $= u_0 C_{g,T} C_p T_g - \lambda \frac{\partial T_g}{\partial z}$	$z = L$ $\frac{\partial C_{g,i}}{\partial z} = 0$ $u_0 = 0$ $\frac{\partial T_g}{\partial z} = 0$
---	---

#### Feed

$z = 0, \text{ inlet}$ $u_{0inlet} C_{inlet,i}$ $= u_0 C_{g,i} - \varepsilon D_{ax} C_{g,T} \frac{\partial y_i}{\partial z}$ $u_{0inlet} C_{inlet,T} = u_0 C_{g,T}$ $u_{0inlet} C_{inlet,T} C_p T_{inlet}$ $= u_0 C_{g,T} C_p T_g - \lambda \frac{\partial T_g}{\partial z}$	$z = L, \text{ outlet}$ $\frac{\partial C_{g,i}}{\partial z} = 0$ $P = P_{outlet}$ $\frac{\partial T_g}{\partial z} = 0$
--	--

#### Counter-current blowdown

$z = 0, \text{ outlet}$ $\frac{\partial C_{g,i}}{\partial z} = 0$ $P = P_{outlet}$ $\frac{\partial T_g}{\partial z} = 0$	$z = L$ $\frac{\partial C_{g,i}}{\partial z} = 0$ $u_0 = 0$ $\frac{\partial T_g}{\partial z} = 0$
--	---

#### Purge

$z = 0, \text{ outlet}$ $\frac{\partial C_{g,i}}{\partial z} = 0$ $P = P_{outlet}$ $\frac{\partial T_g}{\partial z} = 0$	$z = L, \text{ inlet}$ $u_{0inlet} C_{inlet,i}$ $= u_0 C_{g,i} - \varepsilon D_{ax} C_{g,T} \frac{\partial y_i}{\partial z}$ $u_{0inlet} C_{inlet,T} = u_0 C_{g,T}$ $u_{0inlet} C_{inlet,T} C_p T_{inlet}$ $= u_0 C_{g,T} C_p T_g - \lambda \frac{\partial T_g}{\partial z}$
--	--

#### 2.2 Linear Models Identification

In Nogueira et al., (2020(2)) is presented a methodology for the optimization of PSA units concomitantly with the determination of the uncertainty associated with the optimal point. The referred work proposes an optimal operating region, instead of an optimal point. These regions can be translated into linear models to be used in plant representations in the RIHMPC. This procedure opens doors to different practical applications of the optimal operating regions proposed in the referred work.

In the referred work, the authors performed the optimization of the PSA unit studied here. The obtained optimal conditions are presented in Figure 1.

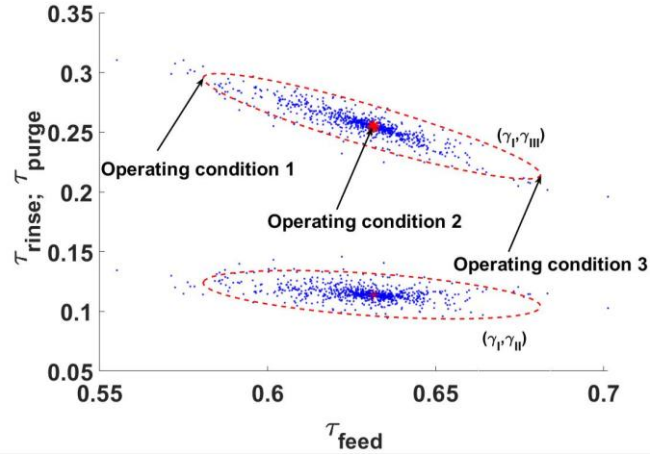


Fig. 1. Optimal operating region, adapted from Nogueira et al., (2020). Each region represents a set of possible optimal operating conditions, where is possible to operate the process keeping the optimal conditions and constraints.

From Figure 1, it can be seen that a wide range of possible optimal conditions can be found where it is efficient to operate the process. That region could hardly be represented solely by a linear model. However, in the scenario where a RIHMPC is used, that region can be divided into subregions and, therefore, multi-models can be identified for each region. In the present case, three subregions were defined, two in each extreme of the optimal area and one in its center. Then, the phenomenological model was used to operate in each of these conditions. Thus, it is possible to identify linear transfer functions for each condition using the reaction steady curve approach (Seborg et al., 2003). Over the cyclic steady state of each

operating condition, it was done a step disturbance of ten percent in each input variable separately. The model response was then used to identify the transfer functions. The sets of manipulated/controlled variables were chosen in accordance with the literature (Regufe et al. 2015). As it is known that the syngas stream will feed a Fischer–Tropsch, the H<sub>2</sub>/CO ratio is an important parameter to be controlled. Furthermore, the CO<sub>2</sub> purity and the CO<sub>2</sub> recovery were also used as controlled variables. As manipulated variables, it was selected the feed step duration, the purge step duration and the rinse step duration. The controlled variables are computed by the phenomenological model as:

$$\frac{H_2}{CO} = \frac{\int_0^{t_{feed}} C_{H_2} u_0|_{z=L} + \int_0^{t_{rinse}} C_{H_2} u_0|_{z=L}}{\int_0^{t_{feed}} C_{CO} u_0|_{z=L} + \int_0^{t_{rinse}} C_{CO} u_0|_{z=L}} \quad (12)$$

$$Pur_{CO_2} =$$

$$\frac{\int_0^{t_{blow}} C_{CO_2} u_0|_{z=0} dt + \int_0^{t_{purge}} C_{CO_2} u_0|_{z=0} dt}{\sum_{i=1}^n [\int_0^{t_{blow}} C_i u_0|_{z=0} dt + \int_0^{t_{purge}} C_i u_0|_{z=0} dt]} \quad (13)$$

$$Rec_{CO_2} = \frac{\int_0^{t_{blow}} C_{CO_2} u_0|_{z=0} dt + \int_0^{t_{purge}} C_{CO_2} u_0|_{z=0} dt - \int_0^{t_{rinse}} C_{CO_2} u_0|_{z=0} dt}{\int_0^{t_{press}} C_{CO_2} u_0|_{z=0} dt + \int_0^{t_{feed}} C_{CO_2} u_0|_{z=0} dt} \quad (14)$$

### 2.3 Robust Model Predictive Control

This work employs the robust MPC proposed by Odloak, (2004), an extension of the work by (Badgwell, 1997) to the output tracking case through a one-step formulation by considering a state-space model in the incremental form of inputs obtained from an analytical expression of the step-response of the system, as well as its guarantee of feasibility for realistic plant/model mismatch by suitable inclusion of a set of slack variables ( $\delta_y$ ), aiming at the enlargement of the domain of attraction of the controller. Therefore, the optimization problem to be solved in the RIHMPC control law at time step  $k$  is expressed as:

$$\begin{aligned} & \min_{\Delta u_k, \delta_{y,k}(\theta_{n=1,\dots,L})} V_k(\theta_N), \\ V_k(\theta_N) = & \sum_{j=0}^m \|y_N(k+j|k) - y_{sp,k} - \delta_{y,k}(\theta_N)\|_{Q_y}^2 + \\ & + \|x_N^d(k+m|k)\|_{Q(\theta_N)}^2 + \\ & + \sum_{j=0}^{m-1} \|\Delta u(k+j|k)\|_R^2 + \|\delta_{y,k}(\theta_N)\|_{S_y}^2 \end{aligned} \quad (15a)$$

s.t.:

$$x_n^s(k+m|k) - y_{sp,k} - \delta_{y,k}(\theta_n) = 0, \quad (15b)$$

$$n = 1, \dots, L$$

$$\begin{aligned} \bar{Q}(\theta_n) = & F^T(\theta_n) \Psi^T Q_y \Psi F(\theta_n) + \\ & + F^T(\theta_n) \bar{Q}(\theta_n) F(\theta_n), \end{aligned} \quad (15c)$$

$$n = 1, \dots, L$$

$$V_k(\theta_n) \leq \tilde{V}_k(\theta_n), n = 1, \dots, L \quad (15d)$$

$$\Delta u_k = [\Delta u(k|k)^T \dots \Delta u(k+m-1|k)^T]^T \in U \quad (15e)$$

$$U = \left\{ \begin{array}{l} \Delta u_{min} \leq \Delta u(k+j|k) \leq \Delta u_{max} \\ \Delta u(k+j|k) = 0, \forall j \geq m \\ u_{min} \leq u(k-1) + \sum_{i=1}^j \Delta u(k+i|k) \leq u_{max} \end{array} \right\} \quad (15f)$$

where  $m$  is the control horizon,  $Q_y$ ,  $R$  and  $S_y$  are weighting matrices (tuning parameters) of the controller.  $\Omega = \{\theta_1, \dots, \theta_L\}$  is a set that contemplates possible operating conditions identified by the optimization, as given in figure 1,  $\theta_n$  denotes a particular operating condition of the plant, i.e.  $\theta_n = \{F_n, B_n^s, B_n^d, n = 1, \dots, L\}$ . The most likely model, the nominal, is referred here as  $\theta_N$ . Even though the objective function is based on a nominal model, Eq. (15d) represents a constraint that is imposed on all the models of  $\Omega$ , in a way to assure the controller robustness. Assuming that  $\Delta u_{k-1}^*$  is the optimal solution of Eq. (11a) at step  $k-1$ ,  $\tilde{V}_k$  is calculated with an inherited solution at time step  $k-1$ , i.e.:

$$\Delta \tilde{u}_k = [\Delta u^*(k|k-1)^T, \dots, \Delta u^*(k+m-2|k-1)^T, 0^T]^T \quad (16)$$

The pseudo-slack variables  $\tilde{\delta}_{y,k}(\theta_{n=1,\dots,L})$  are such that:

$$x_n^s(k+m|k) - y_{sp,k} - \tilde{\delta}_{y,k}(\theta_n) = 0, n = 1, \dots, L \quad (17)$$

The use of the pseudo-slack variables  $\delta_{y,k}(\theta_{n=1,\dots,L})$  is done to accommodate the feedback information of the output  $y(k)$  to all the models in  $\Omega$ .

## 4. RESULTS AND DISCUSSION

The PSA phenomenological model was implemented in gPROMS. To solve the system of partial differential equations, it was used the Orthogonal Collocation in Finite Elements Method (OCFEM) with second-order polynomials in a grid of 150 uniform intervals to perform the spatial discretization of the PDEs which were then solved with DASOLV using a third order orthogonal collocation method (OCFEM). The identification of the linear model was done through MATLAB 2020b, using a gO:MATLAB, an FPI (Foreign Process Interface) event. The simulations were run in a processor Intel® Core™ i5-2400 with a 3.10 GHz CPU. The RAM had an 8.00 GB capacity. The operating conditions are listed in Table 3.

**Table 3 - Operating conditions for the PSA unit simulated by the phenomenological model.**

Bed length (m)	0.323
Bed diameter (m)	0.021
Bed porosity	0.35
Mass of adsorbent (kg)	0.0402
Thermocouple position (m)	0.081/0.191/0.300

Particle radius (mm)	2.00
Crystal radius ( $\mu\text{m}$ )	0.6
Solid density ( $\text{kg m}^{-3}$ )	1450
Apparent particle density ( $\text{kg m}^{-3}$ )	550
Feed flow rate (SLPM)	0.43
Feed composition (%)	30%CO <sub>2</sub> ; 22% CO ; 48% H <sub>2</sub>

For each selected operating condition point shown in Figure 1, a model was identified by the described methodology. Table 4 shows the values of the input variables for each operating condition. In Appendix A, are presented the transfer functions obtained to represent the relationship between the length of the steps: feed ( $t_{\text{feed}}$ ), purge ( $t_{\text{purge}}$ ), rinse ( $t_{\text{rinse}}$ ); and the PSA performance parameters: H<sub>2</sub>/CO ratio, CO<sub>2</sub> purity, CO<sub>2</sub> recovery as output variables of the transfer functions models.

**Table 4 - Operating conditions assumed for the development of the transfer function models.**

	Operating conditions		
	1	2	3
$t_{\text{feed}}$ (s)	463.32	529.37	527.22
$t_{\text{purge}}$ (s)	103.85	87.87	87.87
$t_{\text{rinse}}$ (s)	223.67	205.32	175.74

In order to evaluate the performance of the controller, a simulation was done. The RIHMPC tuning parameters related to the outputs were equal to  $Q_y = [10 \ 5 \ 10]$  and  $S_y = [10^7 \ 10^7 \ 10^7]$  for the ratio, purity and recovery respectively and  $R = [1 \ 10 \ 1]$ . The duration of the simulation was 200 cycles. The performance of the controller was evaluated for the output tracking scenario. In the first test, the controller was activated after the plant reached its cyclic steady state. After 20 cycles, one unmeasured perturbation was added, corresponding to 5% of the feed step duration in order to evaluate the regulatory performance of the RIHMPC. After that, three setpoint changes were done in order to evaluate the performance of the control system during the transition between operating conditions. As the simulation is set on the operating condition 2, the chosen nominal model is the one obtained from that condition whereas the plant is simulated by the model corresponding to the operating condition 3, described in Figure 1. The nominal was chosen in order to assure that there will be a plan/model mismatch, providing a better evaluation of the robust performance of the RIHMPC. Figure 2 shows the simulation results.

It is possible to verify in Figure 2 that the controller was able to drive the process to its setpoint during the output tracking simulation. Furthermore, in the regulatory case, the control was able to bring the controlled variables to the required setpoint. In most of the cases, the controller was able to stabilize the system in less than 5 cycles, though it required considerable time, about 10 cycles, in the ratio control for the last scenario evaluated. This can be a consequence of the trade-off inherent to using a robust controller: as the optimization problem must consider more information to be solved, it finds

conservative control action values. Consequently, more time is required for the controller to track the setpoint for the controlled variables. On the other hand, the controller tuning could be further investigated in order to optimize its performance.

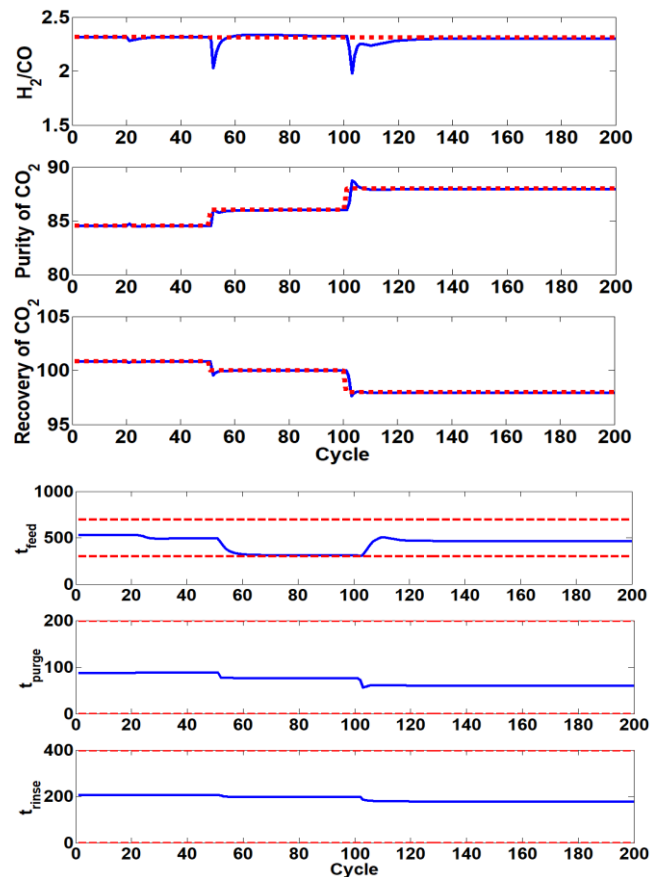


Figure 2 – Process operation for 100 cycles controlled by the proposed RIHMPC. Set of controlled variables, with their setpoints, and manipulated variables, with their respective ranges.

## 5. CONCLUSIONS

This work presented a Robust stabilizing infinite-horizon model predictive controller (RIHMPC) applied in the control of a Pressure Swing Adsorption unit where the syngas purification is processed. The identification of linear models in a multi-plant approach was presented. This was based on the uncertainty evaluation of the unit optimal operating point, which was previously proposed in the literature. The developed controller was tested in a nominal scenario with plant-model mismatch. It was possible to verify that, in both output tracking and regulatory cases, the RIHMPC was able to efficiently keep the process on its setpoints.

## REFERENCES

- Badgwell, T.A., 1997. Robust model predictive control of stable linear systems. *Int. J. Control* 68, 797–818. <https://doi.org/10.1080/002071797223343>
- Da Silva, F.A., Silva, J.A., Rodrigues, A.E., 1999. A General Package for the Simulation of Cyclic Adsorption Processes. *Adsorption* 5, 229–244.

- <https://doi.org/10.1023/A:1008974908427>  
Dias, L.S., Ierapetritou, M.G., 2019. Optimal operation and control of intensified processes — challenges and opportunities. *Curr. Opin. Chem. Eng.* 25, 82–86. <https://doi.org/10.1016/j.coche.2018.12.008>
- Khajuria, H., Pistikopoulos, E.N., 2011. OPTIMIZATION AND CONTROL OF PRESSURE SWING ADSORPTION SYSTEMS.
- M. Mulholland, M.A.L., 2009. PREDICTIVE CONTROL OF PRESSURE SWING ADSORPTION, in: International Conference on Process Control. pp. 65–72.
- Martins, M. a. F., Zanin, A.C., Odloak, D., 2014. Robust model predictive control of an industrial partial combustion fluidized-bed catalytic cracking converter. *Chem. Eng. Res. Des.* 92, 917–930. <https://doi.org/10.1016/j.cherd.2013.08.005>
- Nogueira, Idelfonso B.R., Fontes, R.M., Ribeiro, A.M., Pontes, K. V., Embiruçu, M., Martins, M.A.F., 2020(1). A robustly model predictive control strategy applied in the control of a simulated industrial polyethylene polymerization process. *Comput. Chem. Eng.* 133, 106664. <https://doi.org/10.1016/j.compchemeng.2019.106664>
- Nogueira, Idelfonso B R, Martins, M.A.F., Regufe, M.J., Rodrigues, A.E., Loureiro, J.M., Ribeiro, A.M., 2020(2). Big Data-Based Optimization of a Pressure Swing Adsorption Unit for Syngas Purification: On Mapping Uncertainties from a Metaheuristic Technique. *Ind. Eng. Chem. Res.* *acs.iecr.0c01155*. <https://doi.org/10.1021/acs.iecr.0c01155>
- Odloak, D., 2004. Extended robust model predictive control. *AIChE J.* 50, 1824–1836. <https://doi.org/10.1002/aic.10175>
- Rumbo Morales, J.Y., López López, G., Alvarado Martínez, V.M., Sorcia Vázquez, F. de J., Brizuela Mendoza, J.A., Martínez García, M., 2020. Parametric study and control of a pressure swing adsorption process to separate the water-ethanol mixture under disturbances. *Sep. Purif. Technol.* 236, 116214. <https://doi.org/10.1016/j.seppur.2019.116214>
- Seborg, D.E., Mellichamp, D.A., Edgar, T.F., Doyle III, F.J., 2003. *Process Dynamics and Control*. Wiley, New York.

#### ACKNOWLEDGMENTS

This work was financially supported by: EDUFI Fellowships program, Base Funding - UIDB/50020/2020 of the Associate Laboratory LSRE-LCM - funded by national funds through FCT/MCTES (PIDDAC); FCT – Fundação para a Ciência e Tecnologia under CEEC Institucional program.

Appendix A. Identified models from the nonlinear phenomenological model simulated in gProms.

**Table A.I - Transfer functions identified for operating conditions 1.**

	<i>Ratio H<sub>2</sub>/CO</i>	<i>CO<sub>2</sub> purity</i>	<i>CO<sub>2</sub> recovery</i>
<i>t<sub>feed</sub></i>	$\frac{-0.00071232}{1 + 2 * 4.9282 * 0.0785 * s + (0.0785 * s)^2}$	$\frac{0.032042}{1 + 0.039298 * s}$	$\frac{-0.017768}{1 + 0.86694 * s}$
<i>t<sub>purge</sub></i>	$\frac{0.00073921(1 + 7.4772 * s)}{1 + 2 * 1.1882 * 0.24203 * s + (0.24203 * s)^2}$	$\frac{-0.1559}{1 + 2 * 1.1573 * 0.29997 * s + (0.29997 * s)^2}$	$\frac{-0.0049113}{1 + 2 * 1.5727 * 0.23829 * s + (0.23829 * s)^2}$
<i>t<sub>rinse</sub></i>	$\frac{-0.0024076}{1 + 2 * 2.9777 * 0.14448 * s + (0.14448 * s)^2}$	$\frac{0.11894}{1 + 0.033927 * s}$	$\frac{-0.031047}{1 + 2 * 1.214 * 0.30397 * s + (0.30397 * s)^2}$

**Table A.II - Transfer functions for the operating conditions 2.**

	<i>Ratio H<sub>2</sub>/CO</i>	<i>CO<sub>2</sub> purity</i>	<i>CO<sub>2</sub> recovery</i>
<i>t<sub>feed</sub></i>	$\frac{-0.00060259}{1 + 2 * 2.6735 * 0.11552 * s + (0.11552 * s)^2}$	$\frac{0.025335}{1 + 0.032993 * s}$	$\frac{-0.038022}{1 + 0.86165 * s}$
<i>t<sub>purge</sub></i>	$\frac{0.0008318(1 - 3.9842 * s)}{1 + 2 * 0.62231 * 0.13654 * s + (0.13654 * s)^2}$	$\frac{-0.14465}{1 + 2 * 31.696 * 0.037613 * s + (0.037613 * s)^2}$	$\frac{0.086203}{1 + 0.84253 * s}$
<i>t<sub>rinse</sub></i>	$\frac{-0.002189}{1 + 2 * 2.3997 * 0.13456 * s + (0.13456 * s)^2}$	$\frac{0.11006}{1 + 0.047108 * s}$	$\frac{-0.0074785}{1 + 2 * 19.639 * 0.02456 * s + (0.02456 * s)^2(1 + 250.91 * s)}$

**Table A.III - Transfer functions identified for the operating conditions 3.**

	<i>Ratio H<sub>2</sub>/CO</i>	<i>CO<sub>2</sub> purity</i>	<i>CO<sub>2</sub> recovery</i>
<i>t<sub>feed</sub></i>	$\frac{-0.00091123}{1 + 2 * 2.8731 * 0.1433 * s + (0.1433 * s)^2}$	$\frac{0.031692}{1 + 0.040094 * s}$	$\frac{-0.030928}{1 + 0.79018 * s}$
<i>t<sub>purge</sub></i>	$\frac{0.0009339(1 + 8.4278 * s)}{1 + 2 * 1.3415 * 0.22222 * s + (0.22222 * s)^2}$	$\frac{-0.16059}{1 + 2 * 0.72784 * 0.32545 * s + (0.32545 * s)^2}$	$\frac{0.03672}{1 + 0.74955 * s}$
<i>t<sub>rinse</sub></i>	$\frac{-0.002854}{1 + 2 * 2.9096 * 0.14259 * s + (0.14259 * s)^2}$	$\frac{0.12764}{1 + 0.059151 * s}$	$\frac{-0.020437}{1 + 0.85897 * s}$